Analysis of electric field stimulation of single cardiac muscle cells

Leslie Tung* and Jean-René Borderies‡

*Department of Biomedical Engineering, The Johns Hopkins University School of Medicine, Baltimore, Maryland 21205, USA; and
‡Ecole Nationale Supérieure de Physique de Strasbourg, Strasbourg, France

ABSTRACT Electrical stimulation of cardiac cells by imposed extracellular electric fields results in a transmembrane potential which is highly nonuniform, with one end of the cell depolarized and the other end hyperpolarized along the field direction. To date, the implications of the close proximity of oppositely polarized membranes on excitability have not been explored. In this work we compare the biophysical basis for field stimulation of cells at rest with that for intracellular current injection, using three Luo-Rudy type membrane patches coupled together as a lumped model to represent the cell membrane. Our model shows that cell excitation is a function of the temporal and spatial distribution of ionic currents and transmembrane potential. The extracellular and intracellular forms of stimulation were compared in greater detail for monophasic and symmetric biphasic rectangular pulses, with duration ranging from 0.5 to 10 ms. Strength-duration curves derived for field stimulation show that over a wide range of pulse durations, biphasic waveforms can recruit and activate membrane patches about as effectively as can monophasic waveforms having the same total pulse duration. We find that excitation with biphasic stimulation results from a synergistic, temporal summation of inward currents through the sodium channel in membrane patches at opposite ends of the cell. Furthermore, with both waveform types, a net inward current through the inwardly rectifying potassium channel contributes to initial membrane depolarization. In contrast, models of stimulation by intracellular current injection do not account for the nonuniformity of transmembrane potential and produce substantially different (even contradictory) results for the case of stimulation from rest.

INTRODUCTION

Electrical defibrillation of the heart requires the exposure of the bulk myocardium to a pulsed electric field, or potential gradient (1). It has been suggested that the efficacy of defibrillation is related to the ability of the electrical pulse to excite fully repolarized or partially repolarized tissue (2–4). Classical cable theories for excitable tissues predict a region of tissue depolarization just adjacent to the negative electrode (cathode) and hyperpolarization just adjacent to the positive electrode (anode) for the case in which the electrodes are in contact with the heart. These regional changes can lead to excitation at one or the other electrode, depending on stimulus intensity. However, a recently emerging concept proposes that cardiac excitation can occur in the bulk tissue well away from the stimulus electrodes (5–7). The theoretical basis for this phenomenon is the presence of secondary sources at the junctional resistances of the gap junctions interconnecting adjacent cells (8), which occur at regular periodicities in the electrical structure of the heart (7, 9). As a consequence, during field stimulation or defibrillation it is predicted that the bulk tissue will undergo oscillatory regions of hyperpolarization and depolarization on a cellular length scale (a periodic term), superimposed on a background level of depolarization or hyperpolarization (an aperiodic term) which is greatest adjacent to the stimulus electrodes (6, 8). The potentials arising from the junctional secondary sources result from the isolated nature of the cells (owing to the finite junctional resistance). The single, isolated cardiac cell which we propose to analyze is the limiting case in which the gap junctional resistance becomes infinite, the aperiodic term goes to zero, and the periodic term is maximized.

It is generally accepted that excitation of cardiac membranes from rest occurs when the transmembrane potential reaches a critical threshold potential (the "takeoff potential"), above which the membrane depolarizes in a regenerative fashion. Strength-duration curves have been derived from the charging pattern of a passive membrane (usually a resistive-capacitive membrane) to the takeoff potential by an intracellular current source (10). It is also generally accepted that with field stimulation, the transmembrane potential of individual cells is highly nonuniform with hyperpolarization on one end and depolarization on the other, as demonstrated theoretically (11, 12) and experimentally in noncardiac cell types (13, 14). It is not clear, however, how to integrate these two concepts. A simple approach might be to consider the differential polarization of the field-stimulated cell to be the result of a positive current source on one end and an equally negative current source on the other, as would be the case if the imposed extracellular field were to force current across the membrane and through the cell. One might then suppose that excitation occurs when the depolarized half of the cell reaches the takeoff potential. A difficulty with this explanation lies in identifying the putative current flow in terms of the stimulating electric field. Furthermore, the details of the superposition between the two halves of the cell remain to be specified, and it is unclear to what extent one end of the cell might predominate over the other or what the load-

Address correspondence to Dr. Leslie Tung, Department of Biomedical Engineering, The Johns Hopkins University School of Medicine, 720 Rutland Ave., Baltimore, MD 21205.

ing effect of an oppositely polarized membrane might be. Nevertheless, some investigators have used current-based stimulation to explore the nature of field-based stimulation (3, 15, 16).

An alternative approach which we will adopt is to recognize that the cell is relatively nonconducting compared with the extracellular medium. In this case, the imposed electric field produces a flow of current primarily around the cell, resulting in a gradient in potential along the cell surface. Given that the interior of the cell is essentially isopotential, the surface potential gradient results in a spatially varying transmembrane potential, which then can activate transmembrane currents through voltage-gated ion channels. Both the cell shape and cell orientation with respect to the direction of the applied field are important determinants of the surface potential which develops (11).

To date, the implications of the close proximity of oppositely polarized membranes on excitability have not been explored and are difficult to study experimentally. On the other hand, a theoretical analysis of cells subjected to electric fields is feasible. The intracellular and extracellular potentials have been described for cells with resistive membrane, either analytically for simple geometries of cell shape and orientation (11, 12) or numerically for more generalized geometries (17, 18). Theory also suggests that the hyperpolarized membrane must present an electrical load to the depolarized membrane, analogous to considerations leading to the concept of "liminal length" (19) and electrical load of syncytial tissue (20). In this study, we analyze the extracellular field stimulation of a single cell, using a model consisting of tightly-coupled, oppositely polarized, active patches of membrane. Our goal is to compare this form of stimulation with the more commonly cited case of intracellular current injection.

In the area of defibrillation, one major focus of investigation has been the possible improvement in the efficacy of the defibrillatory shock pulse through the use of biphasic waveforms as an alternative to monophasic waveforms (21), as shown for rectangular or low tilt exponential waveforms (22–24). However, the electrophysiological basis of the tissue response to the two waveforms is still unresolved. In this study we will not analyze the general problem of a shock pulse applied during an arbitrary phase of the cardiac cycle, but rather, applied just at rest. Stimulation from rest in a cellular model offers the advantage of a precisely defined excitation threshold, which may be further characterized by strength-duration curves. The purpose of this study is to compare the predictions of our field-based model against those of models using current injection. We find that with field stimulation, excitability is similar for the two waveforms, in stark contrast to current injection, for which excitability is reduced with biphasic pulses. This finding is only one of many differences which will become apparent from our results. Earlier versions of this study have been presented previously in a project report (25).

MODEL

Electric field stimulation of another excitable tissue, the nerve axon, has been modeled using a one-dimensional cable. The perturbation in the extracellular potential owing to currents generated by the axon can be neglected to a good approximation (26), and therefore, the extracellular potentials along the surface of the axon can be derived from the electric fields through the extracellular volume conductor. These potentials are applied to the cable model as boundary conditions at the extracellular nodes, and an effective "activating" function equal to the spatial gradient of the imposed electric field along the axon has been proposed (27). However, this concept may be an oversimplification (28) because the activating function is only the forcing function and is not necessarily indicative of the total membrane response, owing to interactions between neighboring membrane patches which include homogeneous solutions unrelated to the activating function (29). Also, the membrane has active (nonlinear and time varying) properties that are not linearly related to the activating function. Finally, excitation of the axon by the transverse component of the imposed electric field (similar to the case here for the single cell) is neglected. Therefore, rather than using an activating function, our strategy will be to model the excitation of single heart cells by mapping the surface membrane of the cell onto a one-dimensional cable model and solving directly for the transmembrane potentials and ionic currents, as in the original approach used for myelinated nerve axon (30).

We begin by assuming a prolate spheroidal shape for a cell subjected to a uniform electric field $\vec{\mathbf{E}}$ with magnitude E_o oriented along the long axis of the cell as shown in Fig. 1 *A*. The semimajor axis defined in the *z*-direction is *a*, semiminor axis defined in the *r*-direction ($r^2 = x^2 + y^2$) is *b*, and surface of the cell is given by,

$$\frac{z^2}{a^2} + \frac{r^2}{b^2} = 1. \quad (1)$$

The eccentricity of the spheroid is defined as,

$$\epsilon = \sqrt{1 - b^2/a^2} \quad (0 \le \epsilon \le 1). \quad (2)$$

The extracellular surface potential for this cell shape has been solved analytically by Klee and Plonsey for a resistive membrane with arbitrary cell orientation (11). We utilize here the simplifying condition that the membrane impedance is much higher than that of the bath and cytosolic impedances. The time constant τ over which the surface potential reaches steady state for a step change in field intensity is given below for a spherical cell with radius *a* (12, 31),

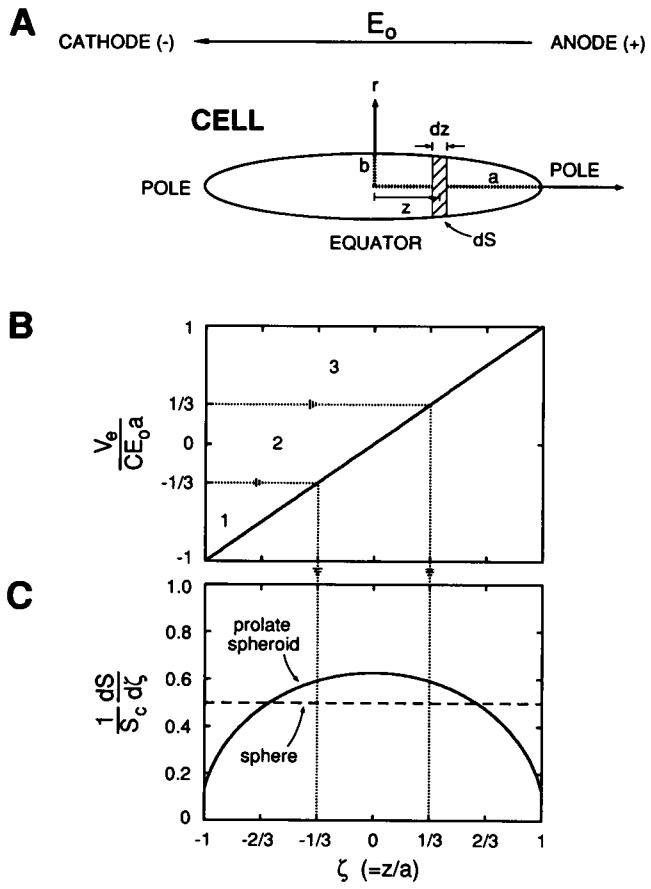

FIGURE 1 Prolate spheroidal cell in uniform electric field. (*A*) The cell has semimajor axis a along the z-direction and semiminor axis b along the r-direction. The cell is subjected to an imposed, uniform electric field. Owing to symmetry, the external surface of an annulus ring of membrane with displacement z from the center of the cell and width of dz is isopotential. (*B*) Surface potential as function of displacement ζ ($=z/a$) along the semimajor axis. For a spheroidal cell, this function is a straight line. (*C*) Relative surface area as a function of displacement ζ. The function $dS/d\zeta$ has been normalized to total cell surface area S_c, so that the area under the curve equals 1. For a prolate spheroidal cell shape (*solid line*, with $b/a = 0.2$), more of the membrane area is weighted towards the equator of the cell and less at the poles. For a spherical cell shape (*dashed line*), the membrane area is equally distributed along ζ.

$$\frac{1}{\tau} = \frac{1}{R_m C_m} + \frac{1}{a(\rho_i + 0.5\rho_e)C_m} \cong \frac{1}{a(\rho_i + 0.5\rho_e)C_m}, \quad (3)$$

where a is the cell radius, ρ_i and ρ_e the intracellular and extracellular specific resistivities, and R_m and C_m the specific membrane resistance and capacitance. τ is on the order of microseconds, as verified by experiments with voltage-sensitive indicator dyes (14), and, thus, we can consider the membrane to be polarized virtually instantaneously following the leading and trailing edges of the stimulus pulse, as we have suggested previously (32). Therefore, we assume the surface potential to be quasi-static. In this case, the membrane patches within parallel rings on the surface (i.e., the shaded area of Fig. 1 *A*) share the same surface potential and may be considered to be homologous. The extracellular surface potential V_e can be determined analytically as a function of distance z and has the form given by Klee and Plonsey (11),

$$V_e = CE_o z, \quad (4)$$

with the coefficient C a function of eccentricity ϵ,

$$C = \frac{2\epsilon^3}{2\epsilon + (1 - \epsilon^2)\ln\frac{1 - \epsilon}{1 + \epsilon}} \quad (1 \le C \le 1.5). \quad (5)$$

In the well known case of a spherical geometry (i.e., $\epsilon = 0$), C becomes 1.5, and V_e assumes a cosine dependence if z is expressed in terms of azimuthal angle (i.e., $z = a\cos\theta$).

The surface area dS of an incremental ring a distance of z from the center of the cell, with width dz and radius r is given by,

$$\begin{aligned} dS &= 2\pi r\sqrt{(dz)^2 + (dr)^2} \\ &= 2\pi r\sqrt{1 + \left(\frac{b^2 z}{a^2 r}\right)^2}\, dz \\ &= 2\pi a^2\sqrt{(1 - \epsilon^2)(1 - (\epsilon\zeta)^2)}\, d\zeta, \end{aligned} \quad (6)$$

using Eqs. 1 and 2, and defining $\zeta = z/a$. V_e and $dS/d\zeta$ are plotted as normalized values in Figs. 1, *B* and *C*. The poles of the cell ($\zeta = \pm 1$) are polarized maximally but subtend the smallest relative surface area.

In this study we will use the simplest topology, a three-patch model with three discrete surface potentials. Although such a representation is a coarse approximation to the continuum of surface potentials (Fig. 1 *B*), it illustrates the essential results with a minimum of complexity, and if desired, can easily be extended to n patches. The surface potential V_e is subdivided into three equal ranges (Fig. 1 *B*). The lumped model representation for the cell membrane corresponding to the three potential ranges is shown in Fig. 2, with a membrane patch to represent each pole (M1 and M3) and a third patch (M2) to represent the cell equator. Because the surface area of each patch is homologous in the discrete representation, a one-dimensional cable model will suffice to represent the spheroidal cell. In general, other three-dimensional axisymmetric cells may be represented by a one-dimensional model provided that the external field is directed along the axis of symmetry. As described earlier, field conditions are imposed as boundary potentials along the extracellular nodes of the model, in contrast to conven-

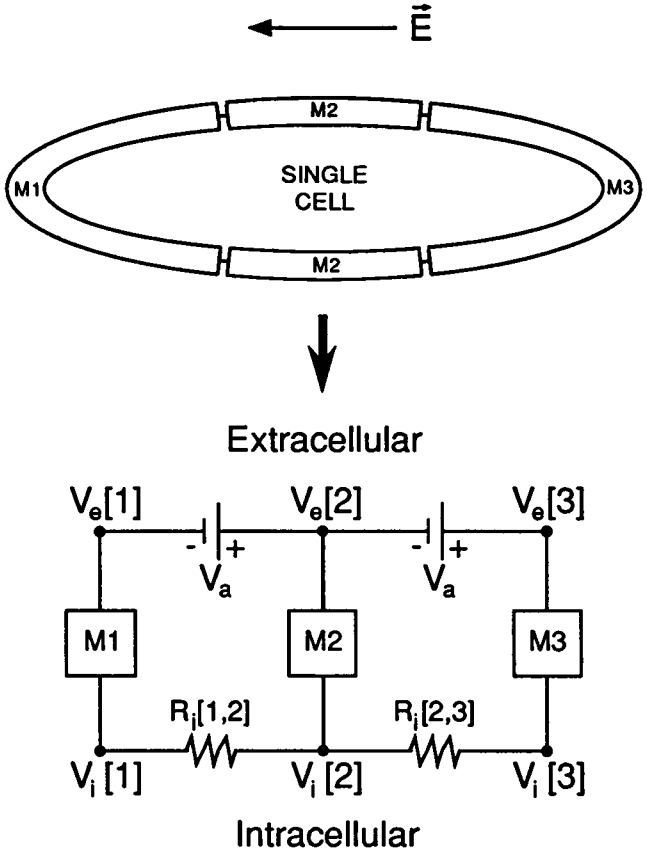

FIGURE 2 The cell membrane is mapped topologically onto a one-dimensional cable model. (*Upper panel*) Patches of cell membrane (M1-M3) along the perimeter of the cell. (*Lower panel*) One-dimensional cable representation. Each membrane patch includes ion channels and lumped capacitance. Intracellular resistances represent pathways for ionic current flow through the cytoplasm. The flow of currents in the cell is driven by gradients in extracellular surface potential, represented by the batteries V_a.

tional models which incorporate transmembrane current sources in parallel with the membrane patches (10). The biophysical properties of each membrane patch are represented by the recent Luo-Rudy model for ventricular cells (33), a six ion channel system which incorporates recent single cell and single channel data. The intracellular resistances $R_i[1, 2]$ and $R_i[2, 3]$ correspond to the term $a\rho_i$ in Eq. 3 and permit a finite charging time of the membrane capacitance as well as propagated activity within the cell. We have omitted extracellular resistances in this model, because in general, $a\rho_e < a\rho_i$. This implies we also neglect the voltage gradients in the extracellular volume conductor arising from transmembrane currents.

The surface areas of each patch are in general, unequal and can be determined as the area under the curve shown in Fig. 1 *C*. The surface area $S(\alpha, a, \epsilon)$ of a membrane patch spanning the axial dimension from $\zeta = -\alpha$ to $\zeta = \alpha$ may be found by integrating Eq. 6:

$$S(\alpha, a, \epsilon) = \int_{-\alpha}^{\alpha} 2\pi a^2 \sqrt{(1-\epsilon^2)(1-(\epsilon\zeta)^2)}\, d\zeta$$

$$= 2\pi a^2 \sqrt{1-\epsilon^2}\left[\alpha \sqrt{1-(\epsilon\alpha)^2} + \frac{1}{\epsilon}\sin^{-1}(\epsilon\alpha)\right]$$

$$(0 \le \alpha \le 1). \quad (7)$$

The total surface area of the cell S_c is given by,

$$S_c = S(1, a, \epsilon) = 2\pi a^2\left[(1-\epsilon^2) + \frac{\sqrt{1-\epsilon^2}}{\epsilon}\sin^{-1}\epsilon\right]. \quad (8)$$

In this study, we will assume $b/a = 0.2$, giving an eccentricity ϵ of 0.980 for which S_c is 0.320 a^2. The surface area $S[2]$ for patch M2 is given by $S(0.333, a, 0.980) = 0.410\ S_c$, and each area $S[1]$ and $S[3]$ for M1 and M3 is 0.295 S_c. The coefficient C in Eq. 4 is 1.059. It can be seen by inspection that in the case of a spherical geometry (*dashed line*, Fig. 1 *C*), $S[1] = S[2] = S[3] = S_c/3$.

A discretized potential gradient along the surface of the cell will be used as the forcing function for the cellular response. We define $V_e[k]$ at the nodes (k = 1, 2, 3) (Fig. 2) to equal the mean values of the 3 potential ranges shown in Fig. 1 *B*, so that:

$$V_e[3] - V_e[2] = V_e[2] - V_e[1] = (2/3)CE_o a \equiv V_a. \quad (9)$$

By symmetry, the potential $V_e[2]$ is also the potential measured at infinity (i.e., zero potential). The transmembrane potentials of the three patches are defined as $V_m[1]$, $V_m[2]$ and $V_m[3]$.

All membrane currents in this study are expressed as current densities (μA/cm^2). The constraint on currents through the patches is given by:

$$\sum_{k=1}^{3} S[k]I_{ion}[k] + \sum_{k=1}^{3} S[k]I_{cap}[k] = S_c(\hat{I}_{ion} + \hat{I}_{cap}) = 0, \quad (10)$$

where $S[k]$ and S_c are the patch and cell surface areas defined earlier, and $I_{ion}[k]$ for each patch is the sum of sodium (I_{Na}), slow inward calcium (I_{si}), time-independent resting potassium (I_{K1}), background potassium (I_b), plateau potassium (I_{Kp}), and time-dependent potassium (I_K) current densities (33),

$$I_{ion}[k] = I_{Na}[k] + I_{si}[k] + I_{K1}[k] + I_b[k] + I_{Kp}[k] + I_K[k]$$
$$(k = 1, 2, 3). \quad (11)$$

$I_{cap}[k]$ is the current density through the specific membrane capacitance $C_m[k]$,

$$I_{cap}[k] = C_m[k] \frac{dV_m[k]}{dt} \quad (k = 1, 2, 3), \tag{12}$$

and $\hat{I}_{ion}$ and $\hat{I}_{cap}$ are the whole cell current densities, with:

$$\begin{aligned} S_c\hat{I}_{ion} &= \sum_{k=1}^{3} S[k]I_{Na}[k] \\ &\quad + \sum_{k=1}^{3} S[k]I_{si}[k] + \sum_{k=1}^{3} S[k]I_{K1}[k] + \sum_{k=1}^{3} S[k]I_b[k] \\ &\quad + \sum_{k=1}^{3} S[k]I_{Kp}[k] + \sum_{k=1}^{3} S[k]I_K[k] \\ &\equiv S_c(\hat{I}_{Na} + \hat{I}_{si} + \hat{I}_{K1} + \hat{I}_b + \hat{I}_{Kp} + \hat{I}_K). \end{aligned} \tag{13}$$

Finally, the intracellular resistances $R_i[1, 2]$ and $R_i[2, 3]$ are estimated as the resistance of a cylindrical plug of intracellular cytoplasm joining the midpoints of patches 1 and 2 (or 2 and 3), with resistivity ρ_i, length of $2a/3$, and radius equal to the value of r at $z = 2a/3$:

$$R_i[1, 2] = R_i[2, 3] = \frac{\rho_i(2a/3)}{\pi(5/9)a^2(1 - \epsilon^2)} = \frac{0.382\rho_i}{a(1 - \epsilon^2)}. \tag{14}$$

In this study we set $R_i[1, 2]$ and $R_i[2, 3]$ to be 350 $k\Omega$, assuming a value of a of approximately 75 μm, with ϵ = 0.98 and ρ_i = 282 Ω-cm (5). These values of intracellular resistance are used in all our simulations, and we find that the intracellular potentials $V_i[1]$, $V_i[2]$, and $V_i[3]$ remain essentially the same during field stimulation. For example, a 100 μA/cm^2 ionic current originating in patch M1 over surface area $S[1] = 0.53 \times 10^{-5}$ cm^2 (a = 75 μm) will result in a voltage drop of only 0.19 mV across $R_i[1, 2]$. The overall intracellular potential will vary, however, with time according to the electrophysiological responses of the membrane patches.

The ionic parameters of the Luo-Rudy model were set at (in mM): Na_i 18, Na_o 140, K_i 145, K_o 5.4, Ca_i 1.784×10^{-4}, Ca_o 1.8; and temperature = 310 K. The membrane response for a given stimulus waveform was computed using a second order Runge-Kutta-Fehlberg algorithm with variable step size no greater than 10 μs (Advanced Computer Simulation Language, Mitchell and Gauthier Associates, Concord, MA) running on a computer workstation (SPARCstation 1, Sun Systems, Mountain View, CA). The excitation threshold is defined in this study as the minimum voltage V_a for which excitation occurs, not to be confused with the transmembrane potential at which regenerative activity occurs (referred to earlier as the takeoff potential), and is determined iteratively to produce an action potential with a latency of ~5 ms after the end of the stimulus pulse. Use of such a lag time results in an extremely precise definition for the excitation threshold. Monophasic and symmetrical biphasic rectangular waveforms were applied to the model of Fig. 2 for cells at a steady-state resting potential of −84.543 mV. Biphasic pulses were symmetrical with a total duration equal to that of the monophasic pulse, which varied from 0.5 to 10 ms.

For comparison, simulations were also performed for stimulation by intracellular current injection. Because the transmembrane potential in this case is uniform along the cell surface (48), a single patch suffices to represent the cell membrane. The membrane is driven by a current source with magnitude I_a (μA/total surface area S_c). In this case, the constraint on current through the membrane is given by:

$$\hat{I}_{ion} + \hat{I}_{cap} = I_a. \tag{15}$$

The minimum current I_a for which excitation occurs is defined as the excitation threshold, and is determined iteratively as before.

RESULTS

Shown in Fig. 3 are simulations of the responses of the three membrane patches to extracellular field stimulation with a 5-ms monophasic rectangular pulse. Voltage traces are shown in the upper row for stimuli just below and just above threshold. The ionic currents I_{Na}, I_{K1}, and I_b for the suprathreshold stimulus are shown in the lower row for each membrane patch; the currents I_{si}, I_{Kp}, and I_K, although included in all our simulations, are negligible until the upstroke of the action potentials and are not shown for the sake of clarity. Note that the transmembrane potentials of the three patches differ during the stimulus pulse; they are time varying with a similar time course but with constant offsets from one another owing to the extracellular potential gradient. Consequently, ionic currents are activated or inactivated to different extents in the three membrane patches. The sum of the ionic currents produces a capacitive current which depolarizes the membrane according to Eqs. 10–12. $V_m[2]$ is particularly significant, because this potential represents that which should be measured with an intracellular electrode relative to a reference electrode located at infinity. During the stimulus pulse a significant I_{Na} is activated in patch M1 (58% of the mean $\hat{I}_{Na}$ occurring later during the upstroke of the action potential). After the stimulus pulse, the transmembrane potentials of the three patches are essentially the same; however, the ionic currents, particularly I_{Na}, will differ owing to the different histories of V_m during the stimulus pulse. Immediately after the trailing edge of the stimulus pulse, I_{Na} decays very quickly in patch M1 and activates very quickly in M3, owing to the very rapid activation time constant (~0.05 ms) at the takeoff potential of ~ −58 mV. During the action potential upstroke, we find that $|I_{Na}[1]| < |I_{Na}[2]| < |I_{Na}[3]|$, owing to differing degrees of inactivation. We also conclude that excitation does not occur when just one part of the membrane becomes positive to

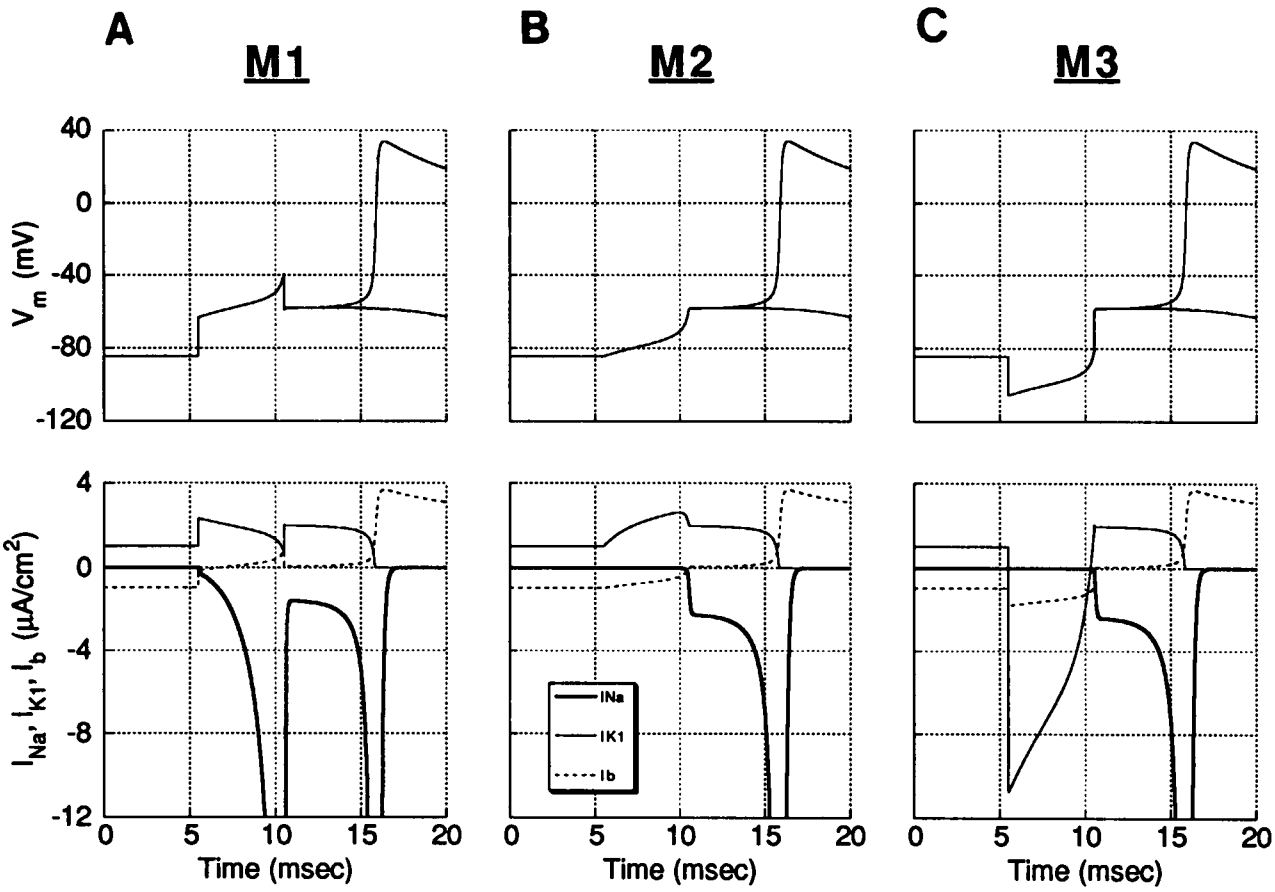

FIGURE 3 Extracellular field stimulation with 5 ms monophasic rectangular pulse. Pulse begins at 5.5 ms. (*A*) Membrane patch M1 at pole of cell facing cathode. (*B*) Membrane patch M2 at equator of cell. (*C*) Membrane patch M3 at pole of cell facing anode. (*Upper row*) The two traces show the transmembrane potential response just above and just below excitation threshold (V_a = 21.188 and 21.189 mV). (*Lower row*) The three traces show the ionic currents I_{Na} (*bold solid trace*), I_{K1} (*light solid trace*), and I_b (*dashed trace*) through each patch for the suprathreshold excitation. The ionic currents I_{si}, I_{Kp}, and I_K do not increase appreciably from the time of rest until after V_m depolarizes to 0 mV, 5.4 ms after the stimulus pulse ends. During this time interval I_{si} over the three patches has reached a maximum value of only -0.27 μA/cm² (in M1), I_{Kp} a maximum value of 0.47 μA/cm² (in M3), and I_K a maximum value of -0.05 μA/cm² (in M3). Therefore these currents have been omitted from this and later figures for the sake of clarity. Peak I_{Na} is offscale in M1 during the pulse (-183.0 μA/cm²) and in M1-M3 during the action potential upstroke (-238.9, -337.1, and -356.9 μA/cm², respectively).

the takeoff potential of ~ −58 mV (as does $V_m[1]$ for the subthreshold pulse), but rather when the entire membrane reaches this threshold (as do $V_m[1]$, $V_m[2]$, and $V_m[3]$) after the end of the stimulus pulse.

The response of the cell membrane to symmetrical biphasic field stimulation can be determined by the same approach used for monophasic stimulation. Here, it will be useful to consider two cases: one in which each phase of the biphasic pulse has the same duration as that for the monophasic pulse, and the other in which the total biphasic pulse duration is the same as for the monophasic pulse (i.e., same total energy). In the first case, the membrane response is shown for 5–5 ms (first phase duration, second phase duration) biphasic stimulation (Fig. 4). Although this pulse has twice the duration of the monophasic pulse considered in Fig. 3, its mode of action has been interpreted in the literature as excitation by the second phase, subject to conditioning of the cell membrane by the first phase (15, 16, 20). I_{Na} in patch M1 undergoes removal of inactivation during phase one and activates during phase two. I_{Na} in patch M3 has the converse behavior, with a slight activation during phase one and both deactivation and removal of inactivation during phase two. Patch M2 depolarizes smoothly and continuously during stimulation but with no significant activation of I_{Na} except at the end of phase two of the stimulus pulse. We find that the biphasic excitation threshold is 13% lower than for monophasic stimulation. However, the amplitudes of I_{Na} in the three patches during the upstroke of the action potential are similar for the two cases of monophasic and biphasic stimulation, demonstrating that phase one of the biphasic pulse has only a minor influence on I_{Na} at that time. Instead, it appears that the effect of the first phase is to partially depolarize the membrane (see $V_m[2]$, *thin arrow*), so that a smaller stimulus amplitude is sufficient during the second phase

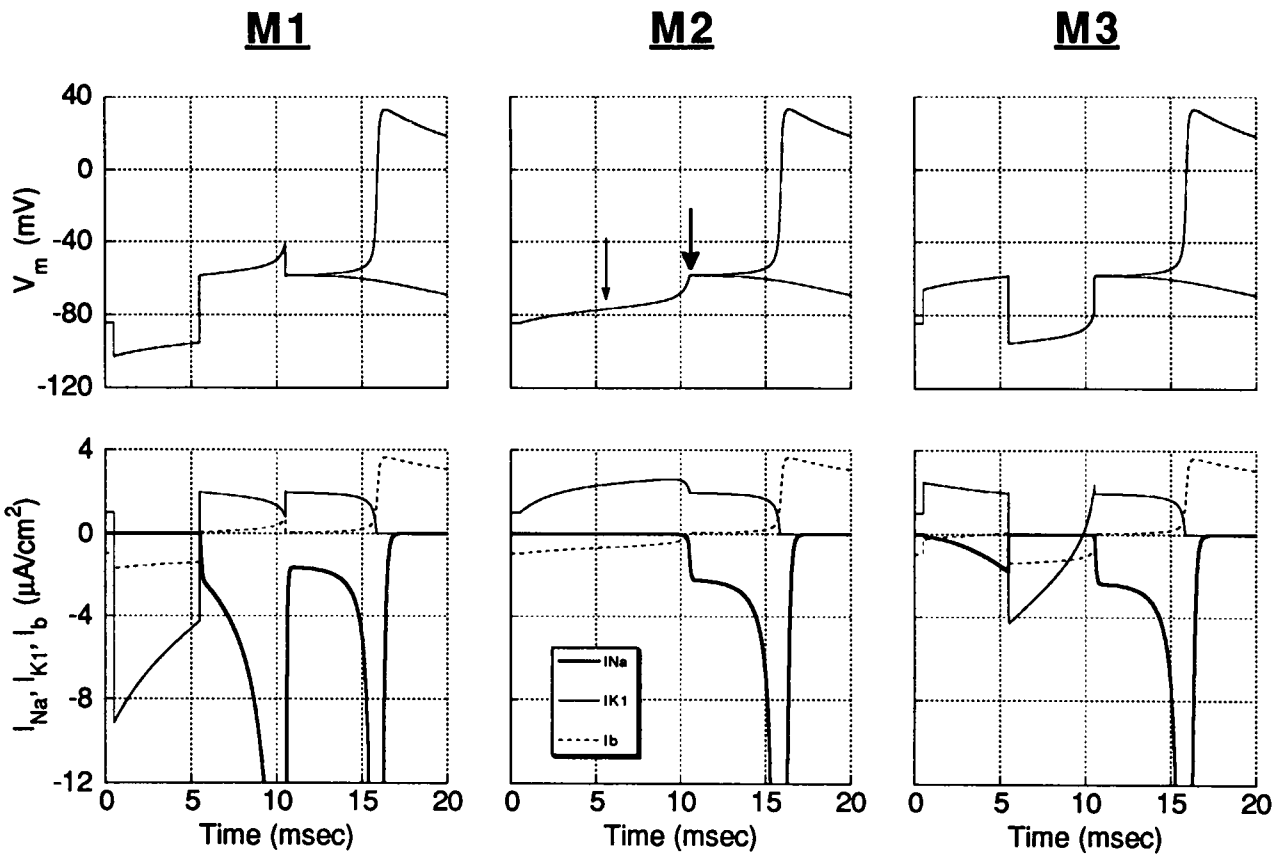

FIGURE 4 Extracellular field stimulation with symmetrical 5–5 ms biphasic rectangular pulse (V_a = 18.492 and 18.493 mV). Pulse begins at 0.5 ms. Upper and lower rows as in Fig. 3. Bold arrow indicates transmembrane takeoff potential; light arrow indicates the level of membrane depolarization at the end of the first stimulus phase. Peak I_{Na} is offscale in M1 during the pulse (−141.1 μA/cm^2) and in M1-M3 during the action potential upstroke (−240.4, −326.1, and −344.7 μA/cm^2, respectively).

to bring the membrane to the takeoff potential, compared with the monophasic pulse. Therefore, under these conditions of rest we can better characterize phase one of the biphasic pulse as a subthreshold excitation pulse which works synergistically with phase two.

The membrane depolarization during phase one of the biphasic pulse arises in part from activation of I_{Na} in patch M3 which, because the activation time constant is ~0.05 ms and rapid inactivation time constant is ~26 ms, follows its steady-state activation curve as the membrane depolarizes. However, depolarization is also a result of a net inward current for the whole cell through the resting potassium channel (I_{K1}), as shown later in Fig. 6. Because this channel rectifies in the inward direction, the currents through the channel sum over the three patches to a negative value and not to zero.

The second case considered here for biphasic field stimulation is for a 2.5–2.5 ms pulse (Fig. 5), which has the same total duration and energy as the 5 ms monophasic pulse. The excitation threshold is slightly lower than for monophasic stimulation (by 1%). Even though the time course (upstroke and overshoot) of the action potential in this case is similar to that elicited with the 5 ms monophasic pulse (Fig. 3), the distribution of I_{Na} among the three patches differs from that for monophasic stimulation, particularly for M1 where I_{Na} is 15% larger. The larger current is necessary because the current must act in only half the time duration of the monophasic pulse to charge the total cell capacitance so as to bring the average membrane potential to the takeoff potential.

Thus far in Figs. 3, 4, and 5, the ionic currents have been displayed individually for each membrane patch to illustrate their differences in activation patterns. These patterns are complex for each ionic channel, and it will be helpful to compare the net (whole cell) ionic currents ($\hat{I}_{Na}$, $\hat{I}_{K1}$, $\hat{I}_b$), summed over all three patches, for each of the three excitatory waveforms: the 5-ms monophasic, 5–5-ms biphasic, and 2.5–2.5-ms biphasic pulse (Fig. 6). Several key features can be noted common to all of the membrane responses. First, the takeoff potentials are similar for all three waveforms (~ −58 mV). Second, $\hat{I}_{Na}$ always activates during the stimulus pulse, but then immediately deactivates after the pulse for a just suprathreshold stimulus. It is this current which is primarily responsible for depolarizing the membrane to the threshold potential. Third, following the onset of the stimulus

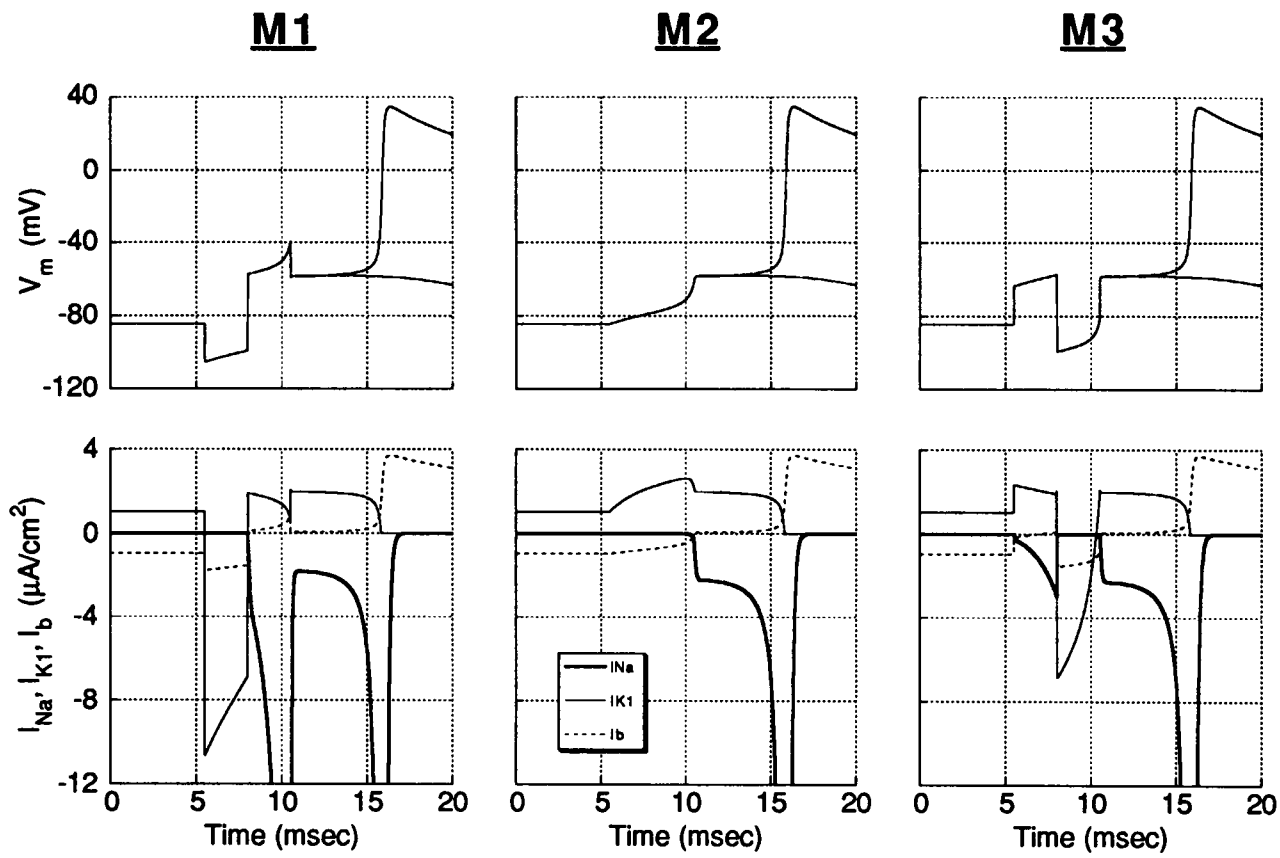

FIGURE 5 Extracellular field stimulation with symmetrical 2.5–2.5 ms biphasic rectangular pulse (V_a = 21.010 and 21.011 mV). Pulse begins at 5.5 ms. Upper and lower rows as in Fig. 3. Peak I_{Na} is offscale in M1 during the pulse (−194.4 μA/cm^2) and in M1-M3 during the action potential upstroke (−274.8, −335.7, and −344.6 μA/cm^2, respectively).

pulse, $\hat{I}_b$ becomes less inward. Especially noteworthy is the finding that $\hat{I}_{K1}$ becomes not only less outward but actually becomes inward and therefore contributes together with $\hat{I}_{Na}$ and $\hat{I}_b$ to membrane depolarization. This result is somewhat surprising, because I_{K1} is normally thought to be outward (repolarizing) as the membrane depolarizes (see, for example, I_{K1}[2] in Fig. 3). Our simulations also show that for the three cases considered (5 ms monophasic, 5–5 ms biphasic, and 2.5–2.5 ms biphasic), $\hat{I}_{K1}$ has peak inward values of −1.5 to −2 μA/cm^2 and does not regain its resting value of 1.03 μA/cm^2 for 4.6–8.0 ms after the onset of stimulation. The biophysical basis for this result can be understood from Figs. 3–5, in which the inward flow of I_{K1} through the hyperpolarized patch following the onset of the stimulus pulse is not counterbalanced by the outward flow of current through the central and depolarized patches, owing to the inwardly rectifying properties of the channel. Fourth, depolarization of the membrane to the takeoff potential can be achieved during the 5–5-ms biphasic pulse with an $\hat{I}_{Na}$ 23% smaller than that during the 5-ms monophasic pulse. Fifth, the activation patterns of the net ionic currents for the 5-ms monophasic and 2.5–2.5-ms biphasic pulses are very similar, despite the different distributions of currents among the three membrane patches as shown in Figs. 3 and 5.

In the next series of simulations, we examined the membrane response to intracellular current stimulation, for the purposes of comparison with extracellular field stimulation. In this case the current responsible for membrane depolarization ($\hat{I}_{cap}$) is provided for by I_a, minus the net outward current $\hat{I}_{ion}$ (Eq. 15). The first case is that of monophasic stimulation (Fig. 7). Unlike with field stimulation, the transmembrane potential is uniform along the cell surface. Furthermore, a polarity dependence is now associated with the stimulus pulse. Positive polarity (i.e., source), monophasic current pulses (*left column*, Fig. 7) are excitatory, but the pattern of activation of $\hat{I}_{Na}$ and $\hat{I}_{K1}$ during the stimulus pulse does not resemble any of the three cases of field stimulation considered previously (Fig. 6). $\hat{I}_{Na}$ does not activate significantly during the stimulus pulse nor does it deactivate immediately following the pulse; furthermore, $\hat{I}_{K1}$ is outward relative to its resting value. However once the stimulus pulse is over and the membrane potential has reached threshold, the time courses of transmembrane potential and ionic currents are similar for both forms of stimulation. Negative polarity (i.e., sink), monophasic

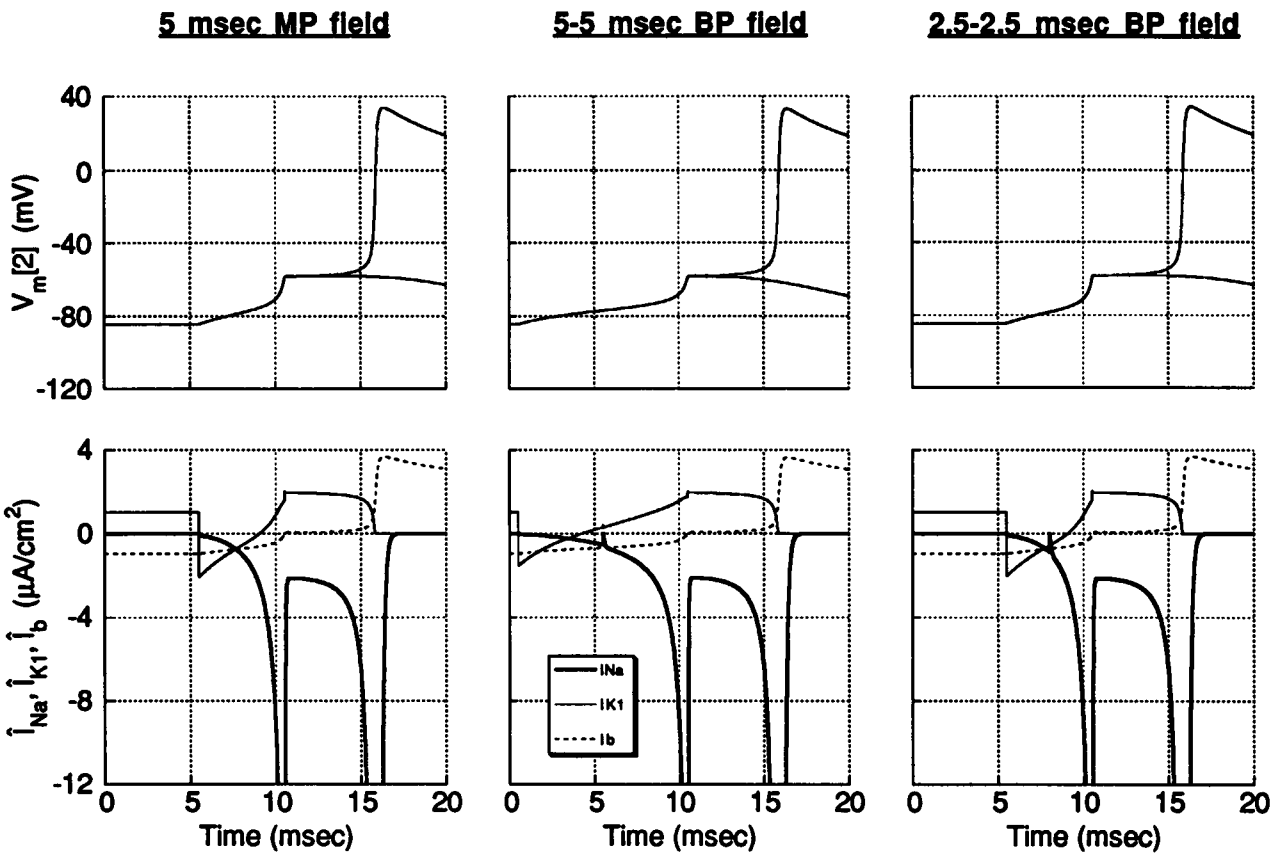

FIGURE 6 Comparison of whole cell membrane currents for field stimulation with a 5 ms monophasic, 5–5 ms biphasic, or 2.5–2.5 ms biphasic pulse. Simulations are the same as those of Figs. 3–5. (*Upper row*) The net transmembrane potential response, $V_m[2]$. (*Lower row*) The net ionic currents for the whole cell, summed over the three membrane patches and normalized for total surface area. Peak $\hat{I}_{Na}$ is offscale at the end of the stimulus pulse (−54.3, −42.0, and −57.6 μA/cm^2) and during the action potential upstroke (−314.0, −306.3, and −320.4 μA/cm^2, respectively for the three cases). $\hat{I}_{K1}$ has peak inward values of −2.06, −1.53, and −2.02 μA/cm^2 and does not regain its resting value of 1.03 μA/cm^2 for 4.58, 7.97, and 4.59 ms respectively, following the onset of stimulation.

current pulses of equal intensity (*right column,* Fig. 7) are not excitatory as has been found to be the case experimentally (34), even if I_a is increased by a factor of 4 over the level shown.

The membrane response to symmetrical biphasic current pulses also can be studied. As in the case for field stimulation, we examine the case for a 5–5-ms biphasic pulse (Fig. 8), for comparison with the 5-ms monophasic pulse. The membrane can be stimulated regardless of whether the initial current phase is positive or negative; also, we find that the stimulus threshold for the biphasic (+/−) pulse is extraordinarily sharp. Stimulation by biphasic pulses, either (+/−) or (−/+), is less effective than by the monophasic (+) pulse alone (I_a is 7 and 25% higher, respectively). If hyperpolarization occurs during phase two (*left column*), the membrane must be brought to a more positive takeoff potential at the end of phase one (*arrow*) than for monophasic stimulation (compare with Fig. 7) so that a larger $\hat{I}_{Na}$ can be activated to offset the hyperpolarizing effect. If hyperpolarization occurs during phase one (*right column*), a larger depolarization is required during phase two to bring the transmembrane potential up to the takeoff potential. Thus, these results suggest that regardless of the order of polarity, the two phases of the biphasic pulse act antagonistically with regard to membrane excitation, and contrast sharply with the case for biphasic field stimulation in which the two phases of the biphasic pulse are synergistic and lead to excitation comparable to that for monophasic stimulation with the same total pulse duration.

The relative efficacy of a particular waveform shape can be quantified in terms of its strength-duration curve (35, 37). Strength-duration curves are shown in Fig. 9 for monophasic and symmetrical biphasic pulses, in which the total duration of the biphasic pulse is defined to be the same as that for the monophasic pulse. Stimulation by extracellular field (*A*) and intracellular current injection (*B*) are plotted for five pulse durations: 0.5, 1, 2, 5, and 10 ms. For extracellular stimulation, biphasic pulses have slightly more efficacy than monophasic pulses at the longer durations, but less efficacy at the shorter durations. If biphasic pulses are compared instead with mono-

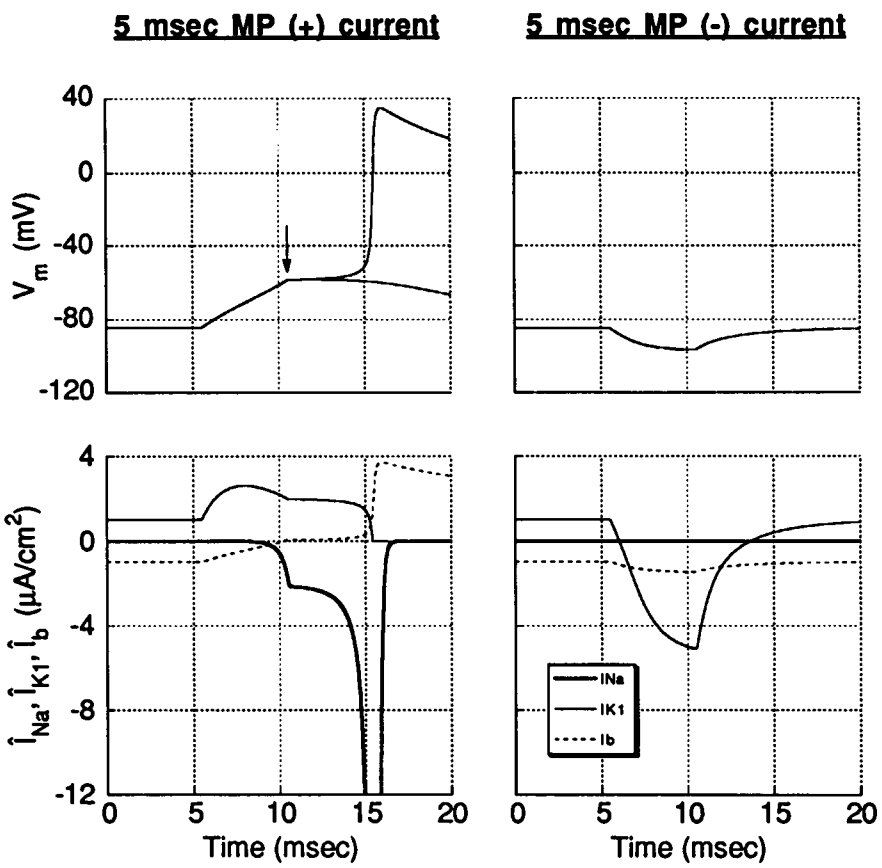

FIGURE 7 Intracellular current stimulation with 5 ms monophasic rectangular pulse. Pulse begins at 5.5 ms. Upper and lower rows as in Fig. 3. (*Left column*) Positive current stimulation (I_a = 6.84 and 6.86 μA/cm^2). Arrow indicates membrane takeoff potential (−58.32 mV). Peak $\hat{I}_{Na}$ is offscale during the action potential upstroke (−323.6 μA/cm^2). (*Right column*) Negative current stimulation (I_a = −6.86 μA/cm^2). An action potential cannot be elicited, even with a stimulus amplitude four times greater than shown.

phasic pulses having half their total duration (i.e., the duration of just one of the two phases), the biphasic pulse is more effective than the monophasic pulse over the entire range of pulse durations. However, these results are markedly reversed for the case of intracellular stimulation. Monophasic (+) pulses are considerably more effective than biphasic pulses, regardless of whether phase one is positive or negative. The difference between excitation thresholds is reduced, but the rank order remains the same, even when biphasic pulses are compared with monophasic pulses having half their total duration.

These results demonstrate that stimulation of cardiac myocytes by imposed electric fields differs fundamentally in many respects from stimulation by intracellular current injection (Figs. 6–9). The qualitative differences between these two forms of electrical stimulation are summarized in Table 1.

DISCUSSION

We have formulated a model of electric field excitation of the cardiac cell which is voltage driven (in terms of the nonuniform surface potential of the cell membrane) unlike conventional models of excitation which are current driven (in terms of a current source charging a passive resistive-capacitive membrane). As described earlier in the introduction, current-based models suffer from a number of difficulties, including the assumption of a uniform membrane potential, absence of any loading effects of one membrane patch on another, and lack of a quantitative relation between the strength of the current source and the intensity of the applied electric field. All of these difficulties are addressed by our model. Despite its simplicity which in this study consists of using only three membrane patches, our model illustrates how the different portions of the cell membrane experience different transmembrane potentials during an imposed electric field and differing degrees of activation or inactivation of ionic currents (Figs. 3–6).

Current vs field stimulation

The major result of this study is that stimulation of cardiac myocytes by imposed, uniform electric fields differs significantly from stimulation by intracellular current injection (Table 1). However, because field stimulation involves a simultaneous hyperpolarization and depolarization of membrane at opposite ends of the cell, we

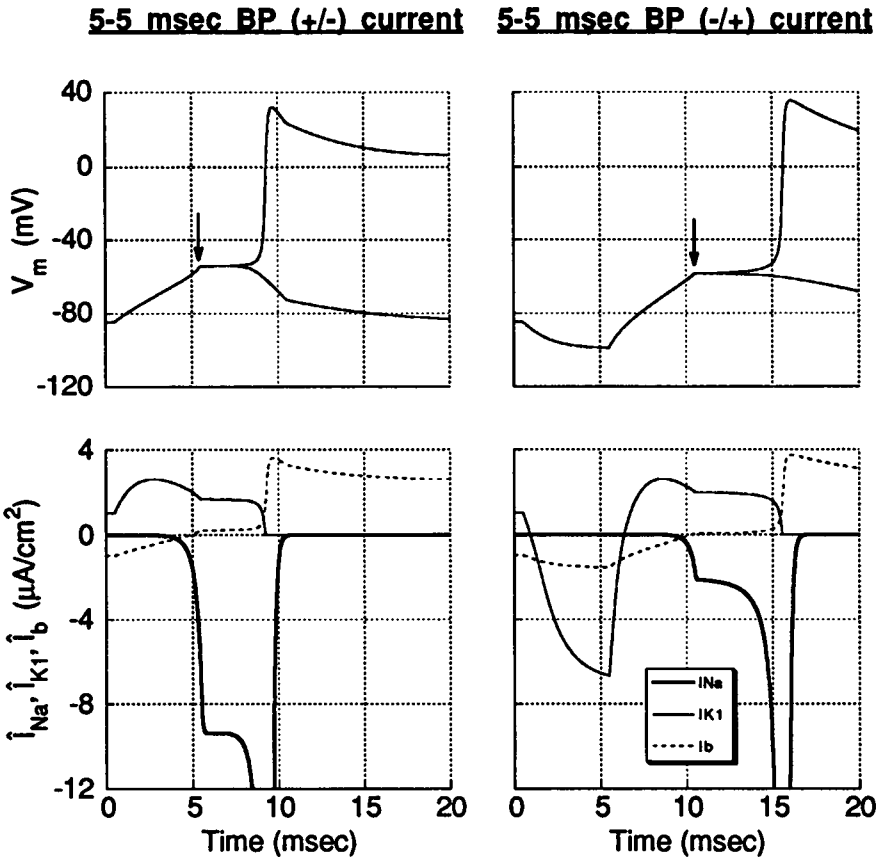

FIGURE 8 Intracellular current stimulation with symmetrical 5–5 ms biphasic rectangular pulse. Pulse begins at 0.5 ms. Upper and lower rows as in Fig. 3. Arrows indicate transmembrane takeoff potentials. (*Left column*) Leading positive phase (I_a = 7.3623 and 7.3624 μA/cm²). Takeoff potential = −54.26 mV. Peak $\hat{I}_{Na}$ is offscale at the end of the stimulus pulse (−321.7 μA/cm²). (*Right column*) Leading negative phase (I_a = 8.56 and 8.59 μA/cm²). Takeoff potential = −58.40 mV. Peak $\hat{I}_{Na}$ is offscale during the action potential upstroke (−330.7 μA/cm²).

return to the question as to whether field stimulation can be understood in terms of a superposition of membrane responses to depolarizing and hyperpolarizing current sources. While this possibility is enticing, we do not believe this to be the case. For example, we can compare the membrane responses of membrane patches M1 and M3 during monophasic field stimulation (Fig. 3) with those for monophasic (+) and (−) current stimulation (Fig. 7). Several points can be made. First, patches M1 and M3 are electrically and tightly coupled, allowing for loading effects of one patch on the other (Fig. 2), whereas the electrophysiological responses of Fig. 7 are those of membrane patches in isolation. Second, the membrane patch potentials $V_m[1]$ and $V_m[3]$ are quite dissimilar from the V_m for (+) and (−) current stimulation, so that the activation patterns of the patch currents must differ. For this reason one would not be able to synthesize the whole cell ionic currents for field stimulation simply as a weighted average of the ionic currents resulting from (+) and (−) current stimulation (compare Figs. 6 and 7). Third and perhaps most significant, the source of depolarizing current which raises the membrane potential from rest to the excitation threshold is very different for field and current stimulation. During field stimulation, the stimulating field supplies no net current into the cell, and therefore a large $\hat{I}_{Na}$ must be activated to supply the depolarizing current. In contrast, during monophasic (+) current stimulation, the stimulus electrode can supply the depolarizing current so that an $\hat{I}_{Na}$ is not necessary. The physical significance is that in one case (field stimulation), charging of the membrane capacitance to the threshold potential is driven by ionic currents (primarily I_{Na}, but also I_{K1}) which are voltage- and time-dependent, whereas in the other (intracellular current injection) the charging is driven primarily by constant current from the stimulus electrode. Ultimately, rigorous experimental tests of our model for extracellular field stimulation may require the use of voltage sensitive dyes applied to single cardiac cells (36), because microelectrode recordings of transmembrane potential are difficult to make reliably during the stimulus pulse (37), and at best will sense only the average membrane potential ($V_m[2]$ in our model).

In this study we have considered the excitation of a single cell by a uniform electric field to be the limiting case for tissue excitation distant from the stimulus electrodes. In this "far field" region, secondary sources produce a periodic hyperpolarized and depolarized response

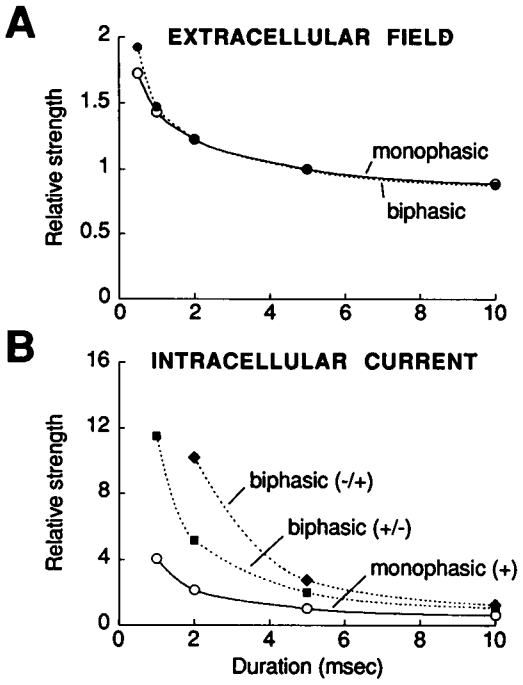

FIGURE 9 Excitation thresholds for extracellular and intracellular stimulation. Thresholds have been normalized to the 5 ms values (21.189 mV for field, 6.86 $\mu A/cm^2$ for current). (*A*) Stimulus thresholds for extracellular monophasic (○) and extracellular biphasic (●) field pulses at five stimulus durations (0.5, 1, 2, 5, and 10 ms). (*B*) Stimulus thresholds for intracellular (+) monophasic (○), intracellular (+/−) biphasic (■), and intracellular (−/+) biphasic (♦) current pulses at the same five stimulus durations. Intensities in each panel have been normalized to the intensity for monophasic stimulation at the 5 ms pulse duration.

(6, 8). However, in the region adjacent to within a few space constants of the stimulus electrode, i.e., the "near field" region, current redistributes between the extracellular and intracellular spaces by traversing across the cell membrane, and results in the aperiodic transmembrane potentials which have been measured in muscle strips (47). These aperiodic potentials, which arise from an extracellular source of current, are similar to those arising from an intracellular source of current with opposite polarity and intensity scaled by the ratio of extracellular to intracellular resistivity (6). Therefore, the extracellular stimulus electrode effectively acts as a form of macroscopic current injection into the cell. The fundamental differences between cellular excitation by extracellular fields and by intracellular current injection (Table 1) could result, then, in different tissue responses in the far and near field regions of the stimulus electrode.

Contribution of I_{K1}

A new finding from our study is that net current through the time-independent inwardly rectifying K channel ($\hat{I}_{K1}$) can act to depolarize the cell membrane, since the inward current through one end of the cell is only partially offset by the outward current through the other end. However, as depolarization progresses, the magnitude of the inward current diminishes and the outward current grows. The currents over the entire cell membrane will balance to zero, for example 3.5 ms after the onset of the 5 ms monophasic pulse (Fig. 6). After this time interval $\hat{I}_{K1}$ becomes outward and subsequently acts to hyperpolarize the cell membrane.

Biphasic vs monophasic stimulation

Extracellular stimulation by rectangular biphasic pulses is of interest because of documented instances of improved efficacy for defibrillation compared with monophasic pulses (22–24, 37). With biphasic field stimulation the first phase has been interpreted as a conditioning prepulse for excitation by the second phase (15, 16, 37). This has been shown to be the case for intracellular (−/+) current stimulation of partially depolarized or incompletely repolarized membranes (15, 16), in which the first phase can enhance excitability through reactivation of $\hat{I}_{Na}$. Our simulations for the case of field stimulation of cells at rest suggest an additional effect of the first phase, as demonstrated in Figs. 4–6. When a 2.5–2.5-ms biphasic pulse is compared with a 5-ms monophasic pulse, the two pulses have essentially the same excitation threshold. Depolarization of $V_m[2]$ to the takeoff potential is achieved in both cases with contributions from $\hat{I}_{Na}$ and $\hat{I}_{K1}$; however, the membrane source of $\hat{I}_{Na}$ and $\hat{I}_{K1}$ differs for the two cases. With monophasic stimulation, $\hat{I}_{Na}$ originates mainly from patch M1 (the patch nearest the cathode), and $\hat{I}_{K1}$ from patch M3 (the patch nearest the an-

TABLE 1 **Stimulation of cardiac cells at normal resting potential by extracellular electric fields, compared with stimulation by intracellular current injection**

	Extracellular field	Intracellular current
Transmembrane potential	Nonuniform	Uniform
Stimulus polarity	Independent*	Dependent
Anodal (−) stimulation	Possible	Not possible
Source of depolarizing current	Ionic currents	Stimulating cathode and ionic currents
$\hat{I}_{Na}$ during pulse	Large amplitude	Small amplitude
$\hat{I}_{Na}$ following pulse	Deactivates, then reactivates‡	Continuously activates‡
$\hat{I}_{K1}$ during pulse	Can be inward	Outward only
Phases of symmetrical biphasic pulse	Synergistic	Antagonistic
Symmetrical biphasic vs monophasic pulses having same total duration	Similar	Less effective

* For uniform field and cells symmetrical about the equator; ‡At threshold.

ode) (Fig. 3). With biphasic stimulation, patches M1 and M3 reverse roles during phases one and two, so that $\hat{I}_{Na}$ originates first from M3, then from M1, and $\hat{I}_{K1}$ originates first from M1, then from M3 (Fig. 5). These findings suggest a synergistic interaction between M1 and M3 across the two phases of the biphasic pulse, as postulated recently to explain the efficacy of biphasic pulses during defibrillation (35). Such an interaction also is consistent with the absence of polarity dependence observed with monophasic field stimulation. The rapid reversal in roles between M1 and M3 is made possible by the time-independent characteristics of I_{K1} and I_b, and the very rapid activation kinetics for I_{Na}; i.e., I_{Na} for patch M1 during phase two can continue where I_{Na} for patch M3 during phase one leaves off. However, for very brief pulses, the effectiveness by which the I_{Na} at the opposite ends of the cell may switch roles becomes rate limited by the voltage-dependent activation kinetics in patch M1 during phase two, and biphasic stimulation becomes less effective compared with monophasic stimulation, as shown in their strength-duration curves at pulse durations < 2.5 ms (Fig. 9 *A*). With these results in mind, we can regard the first phase to act effectively as a subthreshold excitation pulse, and in this sense is a conditioning pulse. On the other hand, models of stimulation via current injection (Fig. 9 *B*) show biphasic pulses to be less effective than monophasic pulses. Experimental studies of field stimulation in the whole heart show no difference during late diastole between rectangular biphasic and monophasic pulses having the same total duration (24), and support the predictions of our field-based model.

The hyperboliclike shape of the strength-duration curves for rectangular monophasic and symmetrical biphasic field stimulation (Fig. 9 *A*) indicates the need to compare the efficacy of the two waveforms for cases in which the total pulse duration of the biphasic pulse is the same as that of the monophasic pulse (23, 24, 38). If for example, a 5-ms monophasic pulse were compared instead with a 5–5 ms biphasic pulse, our model suggests that the biphasic pulse would have a 13% lower threshold. However, much of the apparent improvement in efficacy can be attributed to the inverse nature of the strength-duration curve, in the sense that a pulse with total duration of 10 ms has a lower threshold than a 5-ms pulse. Another point to note is that the strength-duration curve for field stimulation has a chronaxie (time at which the intensity equals twice the rheobase [10]) smaller than that for intracellular current stimulation (Fig. 9). This result is similar to that obtained with non-uniformly polarized (but having the same polarity) membranes in tissue, which have a smaller chronaxie compared with a uniformly polarized membrane (19, 20).

Application to defibrillation

The model presented in this study is but one step towards understanding the biophysical basis for defibrillation, and our results by no means can be generalized to this physiological condition. Given that action potentials are generally asynchronous during fibrillation, only a small fraction of the cells will be at rest at the time of delivery of the shock pulse. Excitation of partially repolarized and relatively refractory myocardium results in a graded response and extension of refractory period (2–4), which halt the activation fronts of fibrillation. The improved efficacy of rectangular biphasic waveforms to defibrillate compared with monophasic waveforms is well established (23, 24), and the basis for the difference has been investigated in terms of the relative abilities of the waveforms to stimulate partially depolarized (15, 16, 37) or relatively refractory (3, 16, 24, 39) tissue or cells.

These conditions can be simulated by our model to provide a basis for the further evaluation of these waveform shapes with respect to field stimulation. A determination of the cellular response under these conditions will help to evaluate the hypothesis that defibrillation is mediated via direct stimulation of the bulk tissue by the shock pulse. However in the final analysis, other factors such as the propensity to reinitiate fibrillation may be critical in determining the efficacy of a given waveform to defibrillate (24, 39). Cellular-based models alone may be inadequate to answer these kinds of questions.

Cell vs tissue

The effects of tissue geometry and cell-to-cell interactions on excitability are not accounted for by single cell models. For example, the electrotonic interactions between cells permit electrical loading (20) and also give rise to an aperiodic or macroscopic variation in transmembrane potential adjacent to the stimulating electrode as described earlier. Another example is given by the bidomain tissue model (40), which suggests that coexisting regions of depolarization and hyperpolarization are formed in the tissue beneath and adjacent to the stimulating electrode, with shapes determined by the anisotropic distribution of conductivities in the extracellular and intracellular domains of the tissue (41). It has been suggested that this structural property of cardiac muscle may account for stimulation at the electrode by anodal pulses (42). Clearly, it will be necessary to exercise caution when extrapolating results from single cells to those of the intact tissue, and to consider carefully the region of interest, whether adjacent to or removed from the stimulating electrodes (i.e., the near field or far field region). Nevertheless, it has been suggested by numerous investigators that it is the dual attributes of depolarization and hyperpolarization of the cardiac membrane on the cellular level, induced in the bulk tissue by the extracellular electric field, which underlies myocardial excitation (3, 5, 6) and defibrillation (2, 6, 7).

REFINEMENTS TO THE MODEL

As with all modeling studies, it is useful to keep in mind the specific assumptions (and therefore, limitations) of

our model, from which refinements can be made in future studies.

Cell shape and number of patches

In this study, the extracellular potential on the surface of the cardiac cell, shaped as a prolate spheroid ($\epsilon = 0.98$), was used as the forcing function. Because the surface potential will be influenced by the eccentricity of the cell (Eq. 3), we have also performed all of the simulations presented in this study for the case of a spherical geometry ($\epsilon = 0$), using a three patch model having equal surface areas (Fig. 1 *C*). Virtually identical results were obtained, both in the distribution of currents among the three patches (Figs. 3–6) as well as in the strength-duration relations for monophasic and biphasic stimulation (Fig. 9 *A*). Therefore, our findings appear to be sufficiently general as to be insensitive to the cell shape as defined by eccentricities in the range of 0–0.98.

Our use of only three discrete surface potentials (and patches) is, of course, a coarse approximation of the continuum of potentials along the surface of the cell (Fig. 1 *B*) and underestimates the maximum potential reached at the poles of the cell. This in turn overestimates the field strength required for excitation. Preliminary simulations using an 11-patch model have verified the expected overestimation (S. Jain and L. Tung, unpublished observations), but have not revealed any significant difference with any of the results obtained with the three-patch model, with the exception of a slightly greater curvature for the strength-duration relation (Fig. 9 *A*). On the other hand, we have considered only surface potential distributions which are symmetric about the cell equator. In general however, the surface potential will not be symmetric and will be influenced by the specific cell shape and orientation with respect to the stimulating field (11). Numerical techniques such as the finite element method can be utilized to determine the surface potential, as implemented for the case of red blood cells in an imposed electric field (18). In the case of a highly asymmetrical distribution of surface potentials, increasing the number of patches in our model may have a greater impact on the results.

Membrane properties

We have used in this study the Luo-Rudy model (33) to represent the biophysical properties of the membrane. In preliminary work using the Beeler-Reuter (43) and modified Beeler-Reuter [Drouhard-Roberge (44)] models, we obtained results similar to those presented in Figs. 3–9 (25), indicating that the general differences between field and current stimulation as shown in Table 1 do not depend on the specific biophysical model used. With those models, we found that the time-dependent current I_{x1}, because of its inwardly rectifying properties, also can contribute to membrane depolarization in much the same way as does I_{K1} in this study.

Imposed electric field

The model presented in this study can be readily extended to describe nonuniform field stimulation, as would be the case for isolated cells in proximity to the stimulating electrode. The surface potential profile will no longer be symmetric about the equator of the cell (an asymmetrical profile also is expected for asymmetrically shaped cells in a uniform field, as described above). Consequently, the excitation response of the cell will depend on the polarity of the field. Cathodal and anodal responses can be expected for monophasic pulses, with an anodal threshold higher than the cathodal threshold. For biphasic pulses, in which the two phases act synergistically, we would expect the excitation threshold to depend less on field polarity than for monophasic pulses. Another point to note is that we have neglected the perturbations in the extracellular potential which arise from the flow of transmembrane currents during the stimulus pulse. The peak amplitudes of these perturbations may be estimated as the product of the peak ionic current, for example 183 $\mu A/cm^2$ in Fig. 3, times the effective extracellular access resistance to the membrane, given by 0.5 $a\rho_e$ in Eq. 3. Assuming a value of 69 Ω-cm for ρ_e (45) and 75 μm for a, the specific access resistance is 0.26 $\Omega\text{-cm}^2$, leading to a potential drop of 47 μV. If desired, this error can be accounted for by inclusion of extracellular resistances in our cable model (Fig. 2) or more generally by a field theoretical approach using Green's theorem (46).

GLOSSARY

$V_e[k]$	extracellular potential at the surface of cell for patch k (k = 1, 2, 3) (mV)
$V_i[k]$	intracellular potential at the surface of cell for patch k (k = 1, 2, 3) (mV)
$V_m[k]$	transmembrane potential ($=V_i[k] - V_e[k]$) of patch k (k = 1, 2, 3) (mV)
$I_{ion}[k]$	total ionic current through cell patch k (k = 1, 2, 3) ($\mu A/cm^2$)
$I_{cap}[k]$	total capacitive current through cell patch k (k = 1, 2, 3) ($\mu A/cm^2$)
$\hat{I}_{ion}$, $\hat{I}_{cap}$	total ionic and capacitive currents for the whole cell ($\mu A/cm^2$)
V_a	magnitude of potential gradient along surface of cell membrane (mV)
I_a	magnitude of intracellular current source ($\mu A/cm^2$)
θ	azimuthal angle between longitudinal axis of cell and electric field axis (rad)
$I_{Na}[k]$, $\hat{I}_{Na}$	current through the sodium channel of the Luo-Rudy model, for patch k (k = 1, 2, 3) and for the whole cell ($\mu A/cm^2$)
$I_{si}[k]$, $\hat{I}_{si}$	current through the slow inward calcium channel of the Luo-Rudy model, for patch k (k = 1, 2, 3) and for the whole cell ($\mu A/cm^2$)
$I_{K1}[k]$, $\hat{I}_{K1}$	current through the time-independent, inwardly rectifying potassium channel of the Luo-Rudy model, for patch k (k = 1, 2, 3) and for the whole cell ($\mu A/cm^2$)

$I_b[k]$, $\hat{I}_b$	current through the background potassium channel of the Luo-Rudy model, for patch k (k = 1, 2, 3) and for the whole cell ($\mu A/cm^2$)
$I_{Kp}[k]$, $\hat{I}_{Kp}$	current through the plateau potassium channel of the Luo-Rudy model, for patch k (k = 1, 2, 3) and for the whole cell ($\mu A/cm^2$)
$I_K[k]$, $\hat{I}_K$	current through the time-dependent potassium channel of the Luo-Rudy model, for patch k (k = 1, 2, 3) and for the whole cell ($\mu A/cm^2$)
a	semimajor axis of cell (cm)
b	semiminor axis of cell (cm)
ϵ	eccentricity of the spheroidal cell
ζ	dimensionless variable indicating displacement along semimajor axis from center of cell (normalized to a)
$d\zeta$	width of incremental surface area of a circular ring on the surface of cell which is equipotential (cm)
ρ_i, ρ_e	intracellular, extracellular specific resistivity (Ω-cm)
$C_m[k]$	specific membrance capacitance for patch k ($\mu F/cm^2$)
$R_i[j, k]$	intracellular coupling resistance between patches j and k ($k\Omega$)
$S[k]$	surface area of patch k (k = 1, 2, 3) (cm^2)
S_c	total surface area of cell (cm^2)

This work was supported by a grant from the Whitaker Foundation to L. Tung. We are grateful to Matthew Fishler for help with our initial simulations, and especially to Sandeep Jain for assisting with our later simulations.

Received for publication 30 October 1991 and in final form 30 March 1992.

REFERENCES

1. Ideker, R. E., P. D. Wolf, C. Alferness, W. Krassowska, and W. M. Smith. 1991. Current concepts for selecting the location, size and shape of defibrillation electrodes. *PACE (Pacing Clin. Electrophysiol.).* 14:227–240.
2. Dillon, S. M. 1991. Optical recordings in the rabbit heart show that defibrillation strength shocks prolong the duration of depolarization and the refractory period. *Circ. Res.* 69:842–856.
3. Swartz, J. F., J. L. Jones, R. E. Jones, and R. Fletcher. 1991. Conditioning prepulse of biphasic defibrillator waveforms enhances refractoriness to fibrillation wavefronts. *Circ. Res.* 68:438–449.
4. Sweeney, R. J., R. M. Gill, and P. R. Reid. 1991. Characterization of refractory period extension by transcardiac shock. *Circulation.* 83:2057–2066.
5. Ideker, R. E., D. W. Frazier, W. Krassowska, P. Chen, and J. M. Wharton. 1990. Physiologic effects of electrical stimulation in cardiac muscle. *In* Electrical Therapy for Cardiac Arrhythmias. S. Saksena and N. Goldschlager, editors. W. B. Saunders Co., Philadelphia. 357–370.
6. Krassowska, W., T. C. Pilkington, and R. E. Ideker. 1987. Periodic conductivity as a mechanism for cardiac stimulation and defibrillation. *IEEE Trans. Biomed. Eng.* 34:555–560.
7. Plonsey, R., R. C. Barr, and F. X. Witkowski. 1991. One-dimensional model of cardiac defibrillation. *Med. Biol. Eng. Comput.* 29:465–469.
8. Plonsey, R., and R. C. Barr. 1986. Inclusion of junction elements in a linear cardiac model through secondary sources: application to defibrillation. *Med. Biol. Eng. Comput.* 24:137–144.
9. Krassowska, W., D. W. Frazier, T. C. Pilkington, and R. E. Ideker. 1990. Potential distribution in three-dimensional periodic myocardium. II. Application to extracellular stimulation. *IEEE Trans. Biomed. Eng.* 37:267–284.
10. Geddes, L. A., and J. D. Bourland. 1985. Tissue stimulation: theoretical considerations and practical applications. *Med. Biol. Eng. Comput.* 23:131–137.
11. Klee, M., and R. Plonsey. 1976. Stimulation of spheroidal cells—the role of cell shape. *IEEE Trans. Biomed. Eng.* 23:347–354.
12. Schwann, H. 1985. Biophysical principles of the interaction of ELF fields with living matter. II. Coupling considerations and forces. *In* Biological Effects and Dosimetry of Static and ELF Electromagnetic Fields. M. Grandolfo, S. M. Michaelson, and A. Rindi, editors. Plenum Publishing Co., New York. 243–271.
13. Gross, D., L. M. Loew, and W. W. Webb. 1986. Optical imaging of cell membrane potential changes induced by applied electric fields. *Biophys. J.* 50:339–348.
14. Kinosita, K., I. Ashikawa, N. Saita, H. Yoshimura, H. Itoh, K. Nagayama, and A. Ikegami. 1988. Electroporation of cell membrane visualized under a pulsed-laser fluorescence microscope. *Biophys. J.* 53:1015–1019.
15. Jones, J. L., and R. E. Jones. 1990. Threshold reduction with biphasic defibrillator waveforms. *J. Electrocardiol.* 23:30–35. (Suppl.)
16. Kavanagh, K. M., H. J. Duff, R. Clark, K. V. Robinson, W. R. Giles, and D. G. Wyse. 1990. Monophasic versus biphasic cardiac stimulation: mechanism of decreased energy requirements. *PACE (Pacing Clin. Electrophysiol.).* 13:1268–1276.
17. Klee, M., and R. Plonsey. 1972. Finite difference solutions for biopotentials of axially symmetric cells. *Biophys. J.* 12:1661–1675.
18. Miller, C., and C. S. Henriquez. 1988. Three-dimensional finite element solution for biopotentials: erythrocyte in an applied field. *IEEE Trans. Biomed. Eng.* 35:712–718.
19. Fozzard, H. A., and M. Schoenberg. 1972. Strength-duration curves in cardiac Purkinje fibres: effects of liminal length and charge distribution. *J. Physiol. (Lond.).* 226:593–618.
20. Joyner, R. W., B. M. Ramza, R. C. Tan, J. Matsuda, and T. T. Do. 1989. Effects of tissue geometry on initiation of a cardiac action potential. *Am. J. Physiol.* 256:H391–H403.
21. Troup, P. J. 1989. Implantable cardioverters and defibrillators. *Curr. Prob. Cardiol.* 14:675–815.
22. Flaker, G. C., J. C. Schuder, W. C. McDaniel, H. Stoeckle, and M. Dbeis. 1988. Superiority of biphasic shocks in the defibrillation of dogs by epicardial patches and catheter electrodes. *Am. Heart. J.* 118:288–291.
23. Schuder, J. C., J. H. Gold, H. Stoeckle, W. C. McDaniel, and K. N. Cheung. 1983. Transthoracic ventricular defibrillation in the 100 kg calf with symmetrical one-cycle bidirectional rectangular wave stimuli. *IEEE Trans. Biomed. Eng.* 30:415–422.
24. Wharton, J. M., V. J. Richard, C. E. Murry, E. G. Dixon, K. A. Reimer, J. Meador, W. M. Smith, and R. E. Ideker. 1990. Electrophysiological effects of monophasic and biphasic stimuli in normal and infarcted dogs. *PACE (Pacing Clin. Electrophysiol.).* 13:1158–1172.
25. Borderies, J. 1991. Simulated ventricular action potential. An analysis of the threshold reduction with biphasic field stimulation. Project report, Ecole Nationale Supérieure de Physique de Strasbourg, Strasbourg, France.
26. Clark, J., and R. Plonsey. 1968. The extracellular potential field of the single active nerve fiber in a volume conductor. *Biophys. J.* 8:842–864.

27. Rattay, F. 1989. Analysis of models for extracellular fiber stimulation. *IEEE Trans. Biomed. Eng.* 36:676–682.

28. Coburn, B. 1989. Neural modeling in electrical stimulation. *Crit. Rev. Biomed. Eng.* 17:133–178.

29. Altman, K. W., and R. Plonsey. 1990. Analysis of excitable cell activation: relative effects of external electrical stimuli. *Med. Biol. Eng. Comput.* 28:574–580.

30. McNeal, D. R. 1976. Analysis of a model for excitation of myelinated nerve. *IEEE Trans. Biomed. Eng.* 23:329–337.

31. Cartee, L. A., and R. Plonsey. 1992. The transient subthreshold response of spherical and cylindrical cell models to extracellular stimulation. *IEEE Trans. Biomed. Eng.* 39:76–85.

32. Tung, L., N. Sliz, and M. R. Mulligan. 1991. Influence of electrical axis of stimulation on excitation of cardiac muscle cells. *Circ. Res.* 69:722–730.

33. Luo, C., and Y. Rudy. 1991. A model of the ventricular cardiac action potential: depolarization, repolarization and their interaction. *Circ. Res.* 68:1501–1526.

34. Hoshi, T., and K. Matsuda. 1962. Excitability cycle of cardiac muscle examined by intracellular stimulation. *Jpn. J. Physiol.* 12:433–446.

35. Feeser, S. A., A. S. L. Tang, K. M. Kavanagh, D. L. Rollins, W. M. Smith, P. D. Wolf, and R. E. Ideker. 1990. Strength-duration and probability of success curves for defibrillation with biphasic waveforms. *Circulation.* 82:2128–2141.

36. Windisch, H., H. Ahammer, P. Schaffer, W. Müller, and B. Koidl. 1990. Optical monitoring of excitation patterns in single cardiomyocytes. *Proc. IEEE 12th Annu. Conf. Eng. Med. Biol. Soc.* 1641.

37. Jones, J. L., R. E. Jones, and G. Balasky. 1987. Improved cardiac cell excitation with symmetrical biphasic defibrillator waveforms. *Am. J. Physiol.* 253:H1418–H1424.

38. Niebauer, M. J., C. F. Babbs, L. A. Geddes, and J. D. Bourland. 1984. Efficacy and safety of the reciprocol pulse defibrillator current waveform. *Med. Biol. Eng. Comput.* 22:28–31.

39. Zhou, X., S. B. Knisley, P. D. Wolf, D. L. Rollins, W. M. Smith, and R. E. Ideker. 1991. Prolongation of repolarization time by electric field stimulation with monophasic and biphasic shocks in open-chest dogs. *Circ. Res.* 68:1761–1767.

40. Plonsey, R. 1989. The use of a bidomain model for the study of excitable media. *Lect. Math. Life. Sci.* 21:123–149.

41. Wikswo, J. P., T. A. Wisialowski, W. A. Altemeier, J. R. Balser, H. A. Kopelman, and D. M. Roden. 1991. Virtual cathode effects during stimulation of cardiac muscle. *Circ. Res.* 68:513–530.

42. Roth, B. J. How the anisotropy of the intracellular and extracellular conductivities influences stimulation of cardiac muscle. *J. Theor. Biol.* In press.

43. Beeler, G. W., and H. Reuter. 1977. Reconstruction of the action potential of ventricular myocardial fibres. *J. Physiol. (Lond.).* 268:177–210.

44. Drouhard, J.-P., and F. A. Roberge. 1987. Revised formulation of the Hodgkin-Huxley representation of the sodium current in cardiac cells. *Comp. Biomed. Res.* 20:333–350.

45. Chapman, R. A., and C. H. Fry. 1978. An analysis of cable properties of frog ventricular myocardium. *J. Physiol. (Lond.).* 283:263–282.

46. Leon, L. J., and F. A. Roberge. 1990. A new cable model formulation based on Green's theorem. *Ann. Biomed. Eng.* 18:1–17.

47. Weidmann, S. 1970. Electrical constants of trabecular muscle from mammalian heart. *J. Physiol. (Lond.).* 210:1041–1054.

48. Hellerstein, D. 1968. Passive membrane potentials. *Biophys. J.* 8:358–379.